Analysis of the iron coatings formed during marcasite and arsenopyrite oxidation at neutral-alkaline conditions

M.P. ASTA[1,2]   **R. PÉREZ-LÓPEZ**[3]   **G. ROMÁN-ROSS**[4]   **V. ILLERA**[2]   **J. CAMA**[5]   **M. COTTE**[6]   **R. TUCOULOU**[6]

[1] **Instituto Andaluz de Ciencias de la Tierra (CSIC-Universidad de Granada)**

Avenida de Las Palmeras 4, Armilla 18100, Granada, Spain.   Asta E-mail: masta@iact.ugr-csic.es; phone number: +34 958230000 ext:190135

[2] **School of Natural Sciences, University of California**

5200 North Lake Road, Merced, CA 95343, USA.

[3] **Departamento de Geología, Universidad de Huelva**

Campus 'El Carmen', 21071, Huelva, Spain

[4] **Amphos 21**

Passeig de Garcia i Faria, 49-51, 1-1, Barcelona, 08019, Spain

[5] **Institute of Environmental Assessment and Water Research (IDAEA), CSIC**

Jordi Girona, 18-26, Barcelona 08034, Spain

[6] **European Synchrotron Facility**

BP -220, Grenoble, Cedex, 28043, France

─┤ **A B S T R A C T** ├─

In order to study the nature of the precipitates formed on arsenopyrite and marcasite after reacting with neutral to alkaline solutions, a combination of techniques including Scanning Electron Microscope-Energy Dispersive Spectroscopy (SEM-EDS), X-ray Photoelectron Spectroscopy (XPS) and synchrotron-based techniques such as micro-X-Ray diffraction (μXRD) and Micro-X-ray Absorption Near Edge Structure (μXANES) have been used. The results showed that the oxidation of marcasite and arsenopyrite under neutral to alkaline conditions leads to the formation of an Fe rich coating which seems to prevent the oxidation of these sulphides. SEM observations confirmed the presence of newly-formed phases after the sulphides reaction under the studied conditions. XPS analysis showed that iron, sulphur and arsenic, in the case of the arsenopyrite, are in oxidized states in the sulphide surfaces. The microscale analysis of the S and Fe speciation performed by μXANES suggested that due to the sulphide oxidation an increase in the oxidation state of those elements took place together with an increase of the sulphate content in the surface layer (grain boundary). Micro-X-ray diffraction results indicated that goethite (α-FeOOH) is the only crystalline newly-formed phase when the reaction occurs at pH 12 whereas at lower pH the products formed on the sulphide surfaces seem to be poorly crystalline and they do not contribute to the diffraction effects in the XRD diagrams.

KEYWORDS │ Sulphide oxidation. Iron phases. Arsenopyrite. Marcasite. Neutral-basic pH.

INTRODUCTION

Oxidation of pyrite and other sulphides of mining wastes leads to generation of acid waters and high concentrations of dissolved metals and metalloids (Acid Mine Drainage, AMD), causing a major environmental problem (Nordstrom and Alpers, 1999).

To minimize the oxidation of sulphide phases present in mine tailings, different treatment methods are used. These methods involve the passivation of the acid-generating material, thus protecting the sulphide surface from water and oxygen. The most common active treatment method in tailings is to increase the pH with an alkaline reagent, such as hydrated lime, precipitating a sludge composed of poorly crystallized Fe-Al oxy-hydroxides/oxy-hydroxysulphates often with significant concentrations of heavy metals and metalloids (*e.g.* copper, zinc, arsenic). This process has several positive effects: i) acidity is neutralized; ii) iron and other metals are removed from the solutions; and iii) the precipitation of Fe-phases on sulphides prevents the grains from further contact with oxygen or other oxidizing agents by blocking the transport of oxidants to the mineral surface.

Among the sulphide minerals, pyrite is the most abundant in natural rocks and mine-wastes and therefore, it has been widely studied. There are numerous investigations on the rates and mechanisms of pyrite oxidation as well as the technologies applied to prevent its oxidation (Nicholson *et al.*, 1988; Nicholson *et al.*, 1990; Evangelou, 1995, 1996, 2001; Evangelou *et al.*, 1998; Vandiviere and Evangelou, 1998; Zhang and Evangelou, 1998; Mylona *et al.*, 2000; Pérez-López *et al.*, 2007; Asta *et al.*, 2008; Huminicki and Rimstidt, 2009). According to previous works (*e.g.* Nicholson *et al.*, 1990, Mylona *et al.*, 2000; Jurjovec *et al.*, 2002; Pérez-López *et al.*, 2007; Huminicki and Rimstdit, 2009), pyrite dissolution at neutral-basic pH values in presence of alkaline substances promotes acid neutralization and depletion of Fe released during oxidation. The Fe(III) produced by the fast oxidation of Fe(II) at alkaline pH (Singer and Stumm, 1970), precipitates as ferric (hydr)oxides, removing Fe (and other metals from solution). This process is known as pyrite microencapsulation (Vandiviere and Evangelou, 1998; Pérez-López *et al.*, 2007). Similarly, the effects of different environmental factors on arsenopyrite oxidative dissolution under neutral to alkaline pH values have been reported in the literature, either related to aqueous chemistry studies (Beattie and Poling, 1987; Hiskey and Sanchez, 1995; Walker *et al.*, 2006; Yu *et al.*, 2007, McKibben *et al.*, 2008; Asta *et al.*, 2010b) or to surface spectroscopic studies based on X-Ray Photoelectron Spectroscopy (XPS) (Buckley and Walker, 1988; Richardson and Vaughan, 1989; Nesbitt *et al.*, 1995; Nesbitt and Muir, 1998; Hacquard *et al.*, 1999;

Mikhlin *et al.*, 2006). In addition, some of those works have studied the precipitates formed during arsenopyrite dissolution (*e.g.* Beattie and Poling, 1987, Hacquard *et al.*, 1999). On the other hand, few studies have focused on the dissolution of marcasite (Mathews and Robins, 1972, 1974; Asta *et al.*, 2010a) and the evolution of marcasite surfaces during oxidation (Rinker *et al.*, 1997; Pratt *et al.*, 1998; Uhlig *et al.*, 2001; Elsetinow *et al.*, 2003; Harmer and Nesbitt, 2004; Asta *et al.*, 2010a).

Many of these previous studies have confirmed the presence of coatings or precipitates on rock and tailing surfaces by using Scanning Electron Microscopy (SEM), X-Ray Diffraction (XRD), and X-Ray Photoelectron Spectroscopy (XPS). In addition, the decrease of iron levels in drainage was often cited as evidence of coating formation and/or iron precipitation. Despite the valuable insights given by the techniques used in previous studies, not many of them provide the capability to evaluate the compositional and mineralogical variation with micrometer spatial resolution combined with solution results. Furthermore, as commented above there are not many studies focused on marcasite dissolution at the pH values of this study.

Therefore, our main goal is to study the nature and characteristics of the marcasite and arsenopyrite surface oxidation layers, which will determine the reactivity of the mineral, its capacity to adsorb aqueous species and the passivation of the acid-generating material under neutral to alkaline conditions similar to those found in treatment methods. With that aim the surface properties of marcasite and arsenopyrite have been investigated by means of a combination of techniques (micro-X-ray absorption near edge structure, XPS and SEM). These techniques allowed us to determine: i) surface stoichiometry compared to the bulk; and ii) nature of the surface products formed during the interactions with neutral and alkaline solutions. In parallel, the evolution of water composition as sulphide dissolution proceeds was also studied.

MATERIALS AND METHODS

Solid characterization

Arsenopyrite and marcasite of this study were obtained from Martinet skarn mineralization (eastern Pyrenees) and from the carbonate-hosted Zn-Pb deposits of Reocín (Cantabria, Spain), respectively. Some arsenopyrite and marcasite fragments were crushed in an agate mortar and sieved to a size fraction powder below 100µm. Initial specific surface area obtained by Brunauer, Emmett and Teller (BET) N_2 adsorption analysis was 0.61±0.07 and 0.9±0.1m^2 g^{-1} for arsenopyrite and marcasite, respectively.

Conventional XRD patterns obtained by powder method using Cu Kα monochromatic radiation showed that the samples consisted of arsenopyrite as the main phase and a minor amount of quartz (approx. 5%) and marcasite with traces of calcite. Electron microprobe analyses were performed on multiple points of the samples using a Cameca SX-50 equipment with an accelerating voltage of 20kV and a beam current of 15nA. The Electron Microprobe analysis (EMP) of the arsenopyrite atomic composition was Fe 33.5±0.1%, As 32.1±0.4% and S 34.4±0.4%. For marcasite the composition was Fe 33.3±0.2% and S 66.7±0.2%. Unreacted and reacted powders for 1500-2000h were examined by SEM using a JEOL JSM-840 microscope and a field-emission scanning microscope Hitachi H-4100FE with intensity current of 15 and 20kV.

X-ray photoelectron spectroscopy

XPS surface examination of initial and reacted samples mounted on carbon conductive tabs was carried out with a Physical Electronics (PHI) 5500 spectrometer using a monochromatic X-ray source with an Al Kα radiation. All the measurements were made in an Ultra High Vacuum (UHV) chamber. Under the measurement conditions used for the analysis of the studied samples the shallowest part of the surface samples were analyzed. Spectra are shown as raw data corrected by adjusting the C1s peak (corresponding to adventitious carbon, to a binding energy of 284.6eV) because of the charge of the sample. In order to obtain the surface stoichiometry the atomic concentrations of arsenic, iron and sulphur were determined from the XPS peak areas divided by atomic sensitivity factors following the Shirley background subtraction (Briggs and Seah, 1990). According to the microprobe analyses, the initial samples were assumed to be perfectly stoichiometric. A deconvolution of the spectra into different components was carried out. Each spectrum was fitted by means of an iterative least-squares procedure with Gaussian bands. The proportion of each surface species was then determined as a function of the areas covered by each band.

Micro-X-ray diffraction and micro-X-ray absorption near edge structure

To identify and characterize the reaction products, synchrotron-based Micro-X-Ray-Diffraction (μXRD) and Micro-X-Ray Absorption near edge structure (μXANES) analyses were performed at the European Synchrotron Radiation Facility in Grenoble (ESRF, France) at beamlines ID18 and ID21, respectively. Information about these beamlines and the instruments used in this study can be found in Somogyi *et al.* (2001), Cotte *et al.* (2006) and Cotte *et al.* (2008). For all X-ray analyses (ID18F and ID21), samples consisted of arsenopyrite and marcasite

polished cross-sections of the reacted powder embedded in an inert resin. Note that the polishing of the samples can disturb the grain coatings. For this reason, the polished sections were previously checked under microscope for pinpointing undisturbed grains.

In the μXRD analyses a double silicon crystal monochromator was used and the excitation energy was fixed at 28keV and the beam was focussed to $5x1.5\mu m^2$ (hor. x ver.). A 2-dimensional CCD camera (refined detector distance 99.5694mm) was used to collect XRD patterns in transmission mode. Debye-Scherrer diffraction rings of the 2D-XRD patterns were unwrapped and integrated versus the azimuthal angle to produce a 1D diffraction pattern (ESRF package Fit2D, Hammersley *et al.*, 1996).

Sulphur and iron μXANES spectra were acquired on the ID21 Scanning X-ray Microscope (SXM). The microscope was operated at S and Fe K-edges (2500 and 7200keV, respectively) using a Si(111) monochromator crystal for S and a Si(220) crystal for Fe. All spectra were collected in X-Ray Fluorescence (XRF) mode with a single-element Silicon Drift Diode (SDD) detector (Bruker AXS, Germany), unfocused beam and beam size $0.21x0.81\mu m^2$ (ver.xhor.) for sulphur and $0.31x1.1\mu m^2$ (ver.xhor.) for iron. For all Fe μXANES data, beam energy was calibrated on an Fe foil with the first edge inflection set to 7112eV. For S XANES the monochromator calibration was done setting the peak value of a gypsum reference to 2482.8eV.

For both elements, in each studied spot, spectra were acquired as the sum of several (up to 10) spectra and averaged. All the spectra were identical during the measurements indicating that there was no radiation damage or beam-induced modifications of the samples in the beamline during the data acquisition. In addition, chemical maps were acquired with 0.2s of acquisition time. Background subtraction and data normalization were performed using the Athena software program (Ravel and Newville, 2005).

To map the distribution of oxidized and reduced states of sulphur, energy difference XRF maps were performed at three different energies (2472.3, 2482.8 and 2500eV), which correspond to maximum absorption in the edge region for different S species. In the case of Fe XRF maps, they were obtained at 7200eV. μXRF spectra were collected in each pixel of the 2D images and were treated with PyMCA software (Solé *et al.*, 2007) and then elemental maps were obtained through a batch treatment.

Dissolution experiments

Dissolution experiments were conducted to evaluate the water evolution during the sulphide dissolution and

to characterize the products of the reaction. With that aim, several experiments were carried out using flow-through reactors (ca. 35mL in volume) fully immersed in a thermostatic water-bath held at a constant temperature of 25ºC under atmospheric conditions and at a pH range from ~7 to ~12. The reaction cells were composed of two chambers, a lower chamber of 33-mm inner diameter and an upper chamber of 26-mm inner diameter. The two chambers were separated by a fine (5μm) nylon mesh, on which 0.5 to 0.8 grams of arsenopyrite or marcasite powder was placed. A schematic sketch of the experimental setting and some more details of the experimental procedure can be found in Asta *et al.* (2010a, b). After the experiments, the reacted samples were collected, rinsed with double-distilled water, dried at room temperature and stored in closed microvials before being analyzed.

Input solutions for the dissolution experiments were prepared by mixing the respective analytical reagents (KH_2PO_4, $NaOH$, $Na_2B_4O_7 \cdot H_2O$ and KCl) and Millipore MQ water (18.2 M$\Omega \cdot$cm). The solution of pH 7.5 was prepared with KH_2PO_4 and $NaOH$, pH 9 solution with $Na_2B_4O_7 \cdot H_2O$, pH 10 solution with $Na_2B_4O_7 \cdot H_2O$ and $NaOH$, and pH 12 solution consisted of KCl and $NaOH$. These solutions were selected for their buffer capacity. Furthermore, in the case of KH_2PO_4 and $NaOH$ its application is especially attractive since both have been proposed for the treatment of sulphide-rich wastes (Evangelou, 2001) and AMD (Johnson and Hallberg, 2005), respectively. With respect to $Na_2B_4O_7 \cdot H_2O$, Pérez-López *et al.* (2007) found that sulphide coatings induced by this reagent are similar to those observed by the application of other alkaline additives commonly used for the AMD treatment, with no influence on the composition of secondary oxidation products.

Total concentrations of As, S and Fe in input and output solutions were analyzed by Inductively Coupled Plasma Atomic Emission Spectroscopy (ICP-AES, Thermo Jarrel-Ash with CID detector and a Perkin Elmer Optima 3200 RL). Detection limits for As, Fe and S were 1.3·10^{-6}, 3.6·10^{-7} and 3.1·10^{-6} mol L^{-1}, respectively.
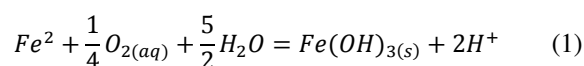
Geochemical calculations

Speciation-solubility calculations were made with the geochemical code PHREEQC (Parkhurst and Appelo, 1999) using the Wateq4f database (Ball and Nordstrom, 2001). The solubility data of lepidocrocite from the Minteq database (Allison *et al.*, 1990) and the thermodynamic data of ferryhidrite from LLNL database (distributed with PHREEQC) have been included in the Wateq4f database to perform the calculations.

RESULTS AND DISCUSSION

Solution chemistry

Figure 1 illustrates the temporal variation in the output concentrations of As and S in arsenopyrite and S in marcasite when the sulphides were leached continuously by circulating solutions in the pH range from 7 to 12. As shown in Figure 1, output concentrations of arsenic in arsenopyrite and sulphur in both minerals were highest at the start of the experiments, subsequently decreasing. Initially high concentrations could be due to the dissolution of microparticles and/or of external, altered layers of the ground mineral (Lasaga, 1998; Acero *et al.*, 2009). Data were collected over a period of 1500-2000h of operation. The released concentrations of arsenic and sulphur for arsenopyrite and sulphur for marcasite decrease notably over the first 200h. Iron was only detected in the first leachates with concentrations in the range of 10-100μM, after which its concentration is below the detection limit of the ICP-AES (3.6·10^{-7}mol L^{-1}) suggesting that Fe was accumulated on the mineral surfaces.

At pH higher than 6, it is expected that Fe(II) released from arsenopyrite and marcasite dissolution oxidizes quickly to Fe(III) (Singer and Stumm, 1970; eq. 1 where Fe(OH)$_3$ represents generic Fe^{3+} precipitates), and that Fe(III)-bearing phases precipitate on arsenopyrite and marcasite surfaces, coating sulphide grains as dissolution proceeds.

$$Fe^2 + \frac{1}{4}O_{2(aq)} + \frac{5}{2}H_2O = Fe(OH)_{3(s)} + 2H^+ \qquad (1)$$

The formation of ferric hydroxide films during the oxidation of arsenopyrite at pH values greater than 7 has been previously reported (*e.g.* Beattie and Poling, 1987; Bhakta *et al.*, 1989). Bhakta *et al.* (1989) observed that the oxide films formed at pH 13.5 seem to be porous and partially hinder the further arsenopyrite oxidation while at pH 7 thin and dense coatings were formed (Koslides and Ciminelli, 1992). Arsenic concentrations in the arsenopyrite output solutions were also stoichiometrically lower than sulphur indicating that part of the arsenic is also being retained in the arsenopyrite surface by sorption or mineral precipitation. Asta *et al.* (2010b) estimated that the amount of arsenic sorbed onto Fe-oxyhydroxide at pH range 4-9 was too low to account for the As that was retained in the experiments, which suggests the formation of an As phase such as scorodite and/or pharmacosiderite ($KFe^{3+}_4(AsO_4)_3(OH)_4 \cdot (6$-$7) \cdot H_2O$) or pitticite ($Fe^{3+}_x(AsO_4)_y(SO_4)_z \cdot nH_2O$) as showed by Beattie and Poling (1987) at pH values greater than 7. Similarly, Hacquard *et al.* (1999) observed the formation of an oxidation layer composed of Fe(III) arsenite and arsenate on the arsenopyrite surface after reacting with a solution of pH 10. These products formed over the sulphide
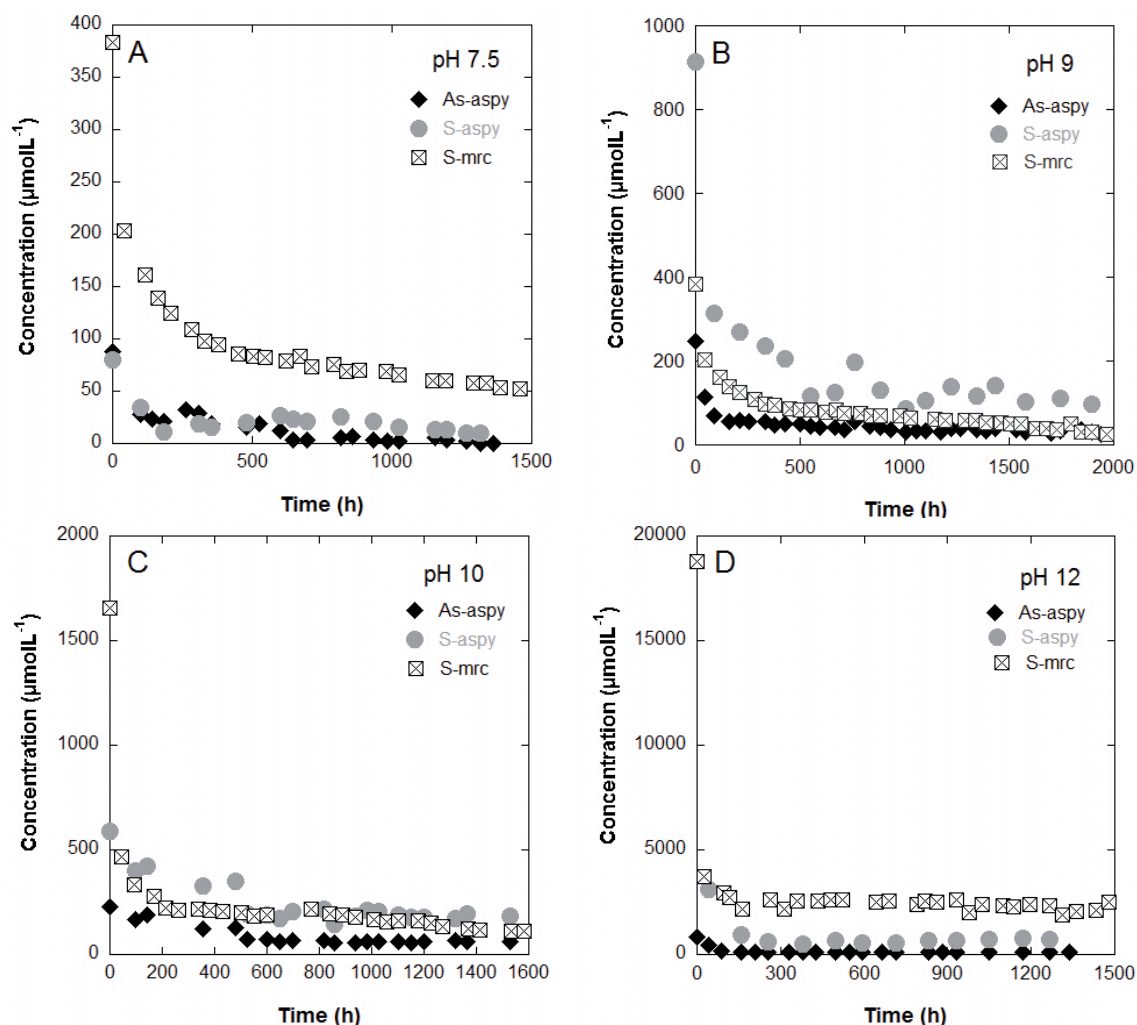
FIGURE 1 | Variation in output As and S concentration in the dissolution experiments of arsenopyrite and marcasite as a function of time at A) pH 7.2-7.5; B) pH 9.1; C) pH 10.0-10.5; D) pH 12.3-12.6, under atmospheric conditions and at a temperature of 25°C. Arsenopyrite data at pH 7.5 and 9.1 are from Asta et al. (2010b).

surfaces block the oxidant transport from solution to the surface, reducing their dissolution rates and therefore the release of the acidity and of contaminant metals to the water (Nicholson *et al.*, 1990; Hood, 1991; Huang and Evangelou, 1993; Evangelou, 1995; Fytas and Evangelou, 1998; Zhang and Evangelou, 1998; Fytas and Evangelou, 1999; Fytas and Bousquet, 2002; Pérez-López *et al.*, 2007; Huminicki and Rimstidt, 2009).

The saturation state of the output solution at the end of the experiments was calculated using the PHREEQC code (Parkhurst and Appelo, 1999) (Table 1). To obtain the saturation indices of the output solutions with respect to Fe, As and S-bearing phases, calculations were run considering congruent dissolution of marcasite and arsenopyrite and calculating Fe and As concentrations based on the sulphur concentrations. According to the PHREEQC modelling results (Table 1), solutions are supersaturated with respect to Fe-oxides and Fe-oxyhydroxides. However, for arsenopyrite all the reacted solutions were undersaturated with respect to scorodite ($FeAsO_4 \cdot 2H_2O$) . It is worth noting that the calculated saturation indexes correspond to the maximum values. Since congruent dissolution was considered, the actual saturation indexes of the experiments were lower than those presented in Table 1.

Scanning electronic microscopy

SEM observations were used to study the surface products formed after the reaction during 1500-2000h of the mineral with solutions with pH values in the range from 7 to 12. SEM photographs of the unreacted sulphides show clean smooth surfaces with sharp edges (Fig. 2A, B) and with some finer fragments over the surface probably as a result from the grinding (Fig. 2B). These surfaces contrast with the images of the oxidized marcasite and arsenopyrite (Fig. 2C-H), which reveal that new precipitates on arsenopyrite and marcasite grains were formed. These

TABLE 1 | Calculated Saturation Index for some mineral phases of reacted solutions with marcasite and arsenopyrite using the PHREEQC code

	Formula	Marcasite pH 7.2	Arsenopyrite pH 7.5	Marcasite pH 10.5	Arsenopyrite pH 10	Marcasite pH 12.3	Arsenopyrite pH 12.4
Goethite	α–FeOOH	9.2	8.2	9.5	8.5	7.3	7.0
Lepidocrocite	γ–FeOOH	5.9	5.1	5.6	6.0	4.9	4.5
Magnetite	Fe_3O_4	13.2	10.2	14.1	11.1	7.6	6.6
Maghemite	γ–Fe_2O_3	9.9	8.0	10.7	8.6	6.2	5.5
Hematite	Fe_2O_3	20.3	18.4	21.1	19.0	16.6	15.9
Ferryhidrite	$Fe(OH)_3$	4.1	3.3	3.8	4.2	3.0	2.7
	$Fe(OH)_{3(am)}$	2.0	1.0	1.4	1.6	0.6	0.3
Strengite	$FePO_4 \cdot 2H_2O$	6.8	5.2	-	-	-	-
Scorodite	$FeAsO_4 \cdot 2H_2O$	-	-5.1	-	-8.1	-	-15.3

secondary precipitates present different degrees of coverage (*i.e.* coating) and some particles were covered by a discontinuous product layer (Fig. 2C, D, F; see for example points 1 and 2 of Fig. 2D) whereas others display a more continuous coating (Fig. 2E,G, H). In addition, Figure 2G and H of marcasite and arsenopyrite reacted samples at pH 12 show needle-like (acicular) particles of sub-micrometer size, which could be goethite crystals since this mineral presents typically needle-shape morphology.

The composition of the precipitates formed after the reaction with marcasite was analyzed by Scanning Electron Microscope-Energy Dispersive Spectroscopy (SEM-EDS) at different locations of the samples (Fig. 3). The results reveal that the composition of the precipitates formed after the reaction is heterogeneous with zones enriched in Ca or Fe, suggesting that the coatings are mainly formed by these elements. In contrast, the initial samples are primarily composed of Fe and S. In the case of the EDS analysis after the reaction at pH~7 with KH_2PO_4, the spectra also show the presence of phosphorous and potassium in the precipitates, which could suggest the formation of an iron-potassium phosphate complex coating as previously reported by Nyavor and Egiebor (1995) or Evangelou (1996). However, no direct evidence supporting the presence of a phosphate phase has been found and this interpretation is speculative at present.

The formation of these precipitates and coatings blocks oxidant transport from the solution to the sulphide surfaces producing a decrease in iron, arsenic (in the case of arsenopyrite) and sulphur released over time, as shown in Figure 1, and a final surface passivation (*e.g.* Pérez-López *et al.*, 2007; Huminicki and Rimstidt, 2009; Asta *et al.*, 2010b).

Micro-X-ray diffraction

The Micro-X-Ray Diffraction (μXRD) technique was also used to characterize the precipitates formed after the marcasite reaction with neutral to alkaline solutions. The diffractograms show that the most intense peaks are attributable to every marcasite sample. Goethite (α-FeOOH)

is the only crystalline newly-formed phase that is clearly identified in the XRD patterns of the experiments at pH 12 (Fig. 4). In the remaining experiments, no obvious crystalline reaction products were observed. Instead, poorly crystalline or amorphous iron phases must be present since they do not contribute to the diffraction effects in the XRD diagrams. A diffraction peak around 2.54Å in some patterns suggests the possible presence of feroxyhite (δ-FeOOH) and/or hematite (α-Fe_2O_3) in the samples reacted at pH 10. The existence of feroxyhite and hematite is consistent with some previous studies that observed both secondary products after the reaction of pyrite at neutral-alkaline pH values (Caldeira *et al.*, 2003). Whether goethite observed at pH 12 precipitates directly from the solution after the reaction or is the product of transformation of less crystalline iron phases is still in contention. For instance, the formation of goethite from ferrihydrite in alkaline media is plausible; in addition the ferrihydrite transformation to more stable goethite is favoured by increasing the pH (Cornell and Schwertmann, 1996).

Iron phosphate phases could be also present at neutral pH as a result of the reaction of marcasite with KH_2PO_4, which is reasonable considering the SEM-EDS results (Fig. 3). In fact, ferric phosphate coatings to diminish the oxidation rate were previously precipitated on sulphide surfaces by leaching with phosphate solutions (Evangelou, 2001; Belzile *et al.*, 2004). However, despite the fact that both phosphate (in samples reacted at pH~7) and sulphate (mainly in samples reacted at pH 10 and 12) were detected in SEM-EDS spectra of the reacted samples, no phosphate or sulphate phases have been found by means of the μXRD analysis. That could be due to the presence of phosphate and sulphate in amorphous phases or in a very low percentage and therefore no detectable by XRD.

X-ray photoelectron spectroscopy

Fe2p$_{3/2}$ spectra and O1s spectra

The Fe2p$_{3/2}$ spectrum of marcasite and arsenopyrite after the reaction is shown in Figure 5A. When those minerals react with solutions at neutral-basic pH, a layer
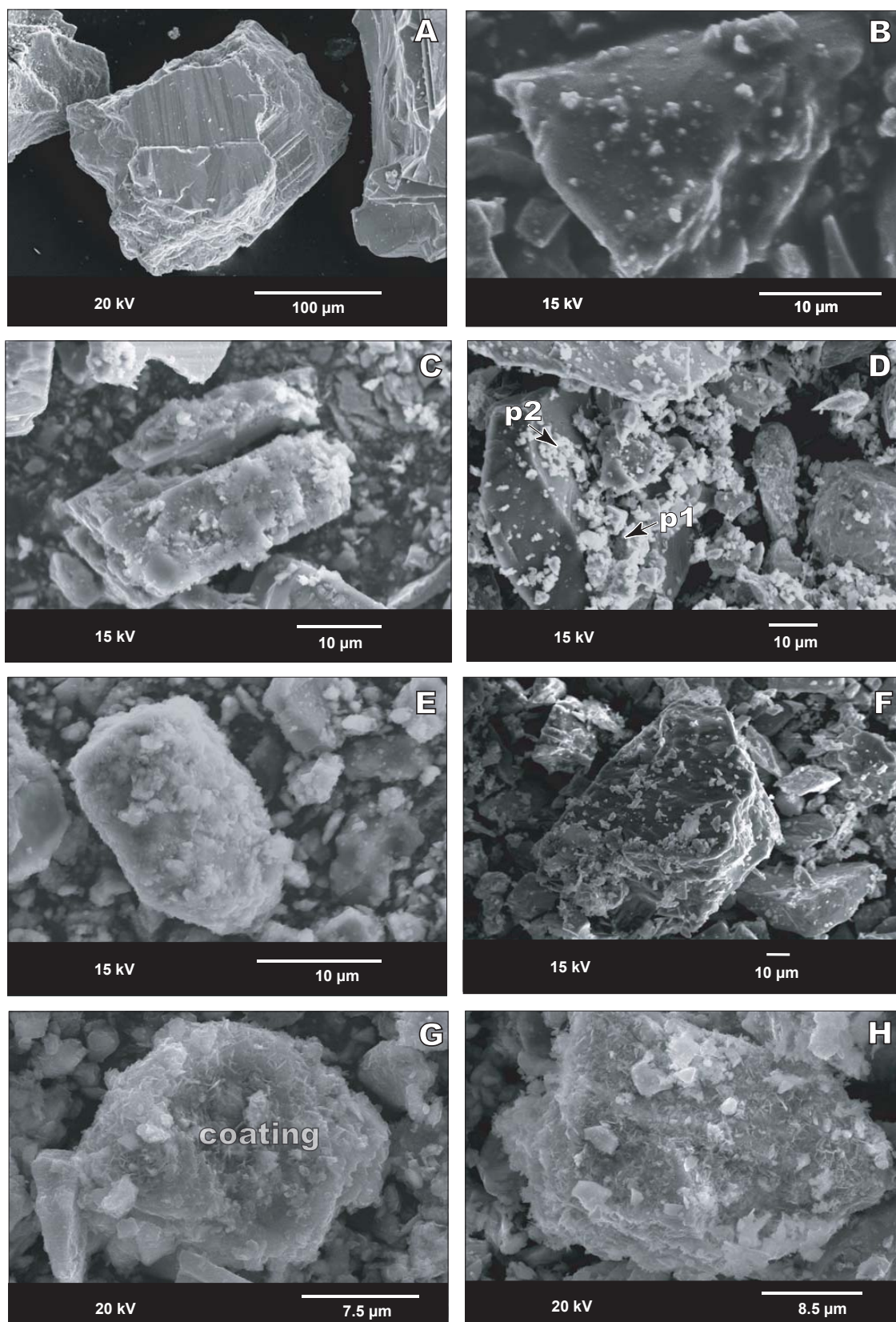
FIGURE 2 | SEM images of A) freshly ground and sieved marcasite; B) arsenopyrite before experiments; and after reaction at pH 7.4-7.5 C) marcasite, D) arsenopyrite; pH 9.8-9.9 E) marcasite, F) arsenopyrite; pH 12.4-12.6 G) marcasite, H) arsenopyrite during 1500-2000h.
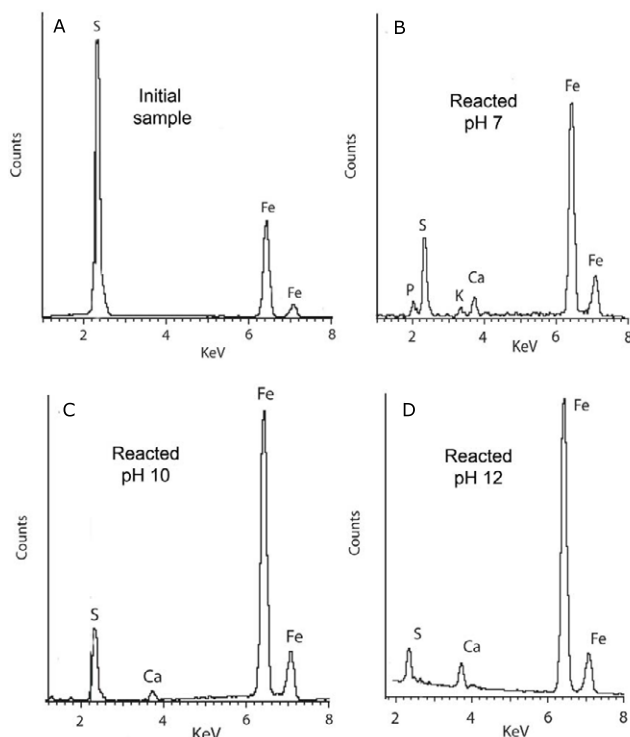
FIGURE 3 | Energy dispersive spectroscopy spectra of A) unreacted maracasite; B) maracasite after reacting with solutions of pH~7; C) pH~10 and D) pH~12.

is formed in the surface as revealed by SEM observations. The broad peak detected in the range of 710.7 to 711.1eV in arsenopyrite and at 711.0 to 711.5eV in marcasite can be interpreted as Fe(III)-O bonds (Nesbitt and Muir, 1998, Hacquard *et al.*, 1999). For example, maximum Fe2p$_{3/2}$ peaks near 710.5eV and 711.5eV have been interpreted as hematite or maghemite (αFe$_2$O$_3$ and γFe$_2$O$_3$; McIntyre and Zeratuk, 1977) and goethite (Nesbitt and Muir, 1998) respectively. The broadness of these peaks is probably suggesting the existence of a variety of Fe(III) compounds. This overlayer could be a mixture of different Fe(III)-oxides together with Fe(III)-sulphates values since the S2p results revealed an important contribution of the sulphate signal at 168-169eV at the highest pH values (see S2p spectra section below). No significant contribution of the main peak at Fe(II) of FeS$_2$ or of FeAsS at binding energies of 707.05 and 707.42eV (Hacquard *et al.*, 1999), respectively, has been observed indicating that the pristine sulphide surface is not exposed and that the presence of Fe(III) precipitates is dominant over the surface.

The O1s spectra are shown in Figure 5B. Similar to previous studies, our fitting procedure used oxide oxygen at 529.2-530.1eV, hydroxide at 530.7-531.6eV and attached H$_2$O at 532.2eV (Harvey *et al.*, 1981; Ferris *et al.*, 1989; Scheidegger *et al.*, 1993; Bonnissel-Gissinger *et al.*, 1998; Nesbitt and Muir, 1998) as components. The

presence of sulphate oxygen overlaps the binding energy of OH– (Nesbitt and Muir, 1998). Both O1s and Fe2p$_{3/2}$ data support the presence of Fe(III)-oxyhydroxide in the surface of the arsenopyrite and marcasite reacted samples.

S2p spectra

S2p spectra of marcasite and arsenopyrite are shown in Figure 6 as a function of the reacted pH. An examination of the S2p spectrum of marcasite reacted at pH 7, 10 and 12 (Fig. 6A) indicate the existence of three possible species at binding energies of 162.8-163.4eV and 168.4-168.7eV. Based on the binding energies (BE) values reported in previous studies (Buckley and Woods, 1985a; Mycroft *et al.* 1990; Nesbitt and Muir, 1994, 1998; Pratt *et al.* 1994; Nesbitt *et al.*, 1995; Bonnissel-Gissinger *et al.*, 1998; Hacquard *et al.*, 1999; Uhlig *et al.*, 2001; Elsetinow *et al.*, 2003) the lowest value of 162.8eV found in the samples reacted at pH 7 and 10 was assigned to the disulphide region (S$_2^{2-}$ of FeS$_2$). The species at binding energy of 163.4eV of the reacted sample at pH 12 is in the polysulphides region (S$_{n2-}$ where n$\geq$2). The peak at the highest energy, in the region of 168.3-168.6eV, required to produce a good fit to the S2p spectra corresponds to the region of sulphate (Nesbitt *et al.*, 1995). The S2p spectrum of the reacted arsenopyrite (Fig. 6B) indicates the existence of two possible species at BE of approximately 163.7-164.1eV, and 168.5-168.9eV in the range of pH studied. These binding energies were identified as polysulphides, and sulphate, respectively, according to the values reported in earlier studies (Buckley and Woods, 1985a; Mycroft *et al.*, 1990; Nesbitt and Muir, 1994, 1998; Pratt *et al.*, 1994; Nesbitt *et al.*, 1995; Hacquard *et al.*, 1999).

The marcasite and arsenopyrite surfaces show some changes when reacted at different pH values. In the case of marcasite the S2p spectra of the reacted sample at pH 7 and 10 are composed of disulphides and sulphates. At
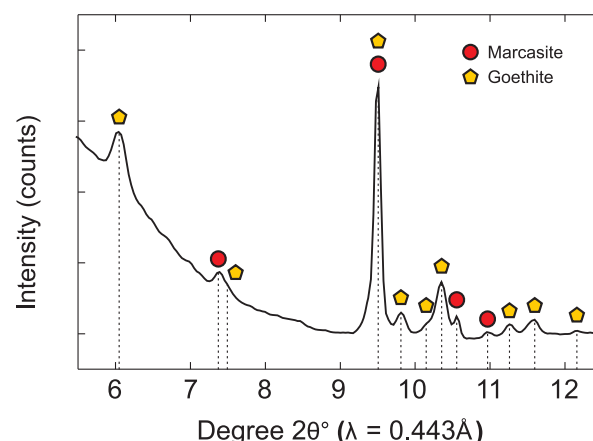

FIGURE 4 | Synchrotron-based μXRD spectrum after integration of data with package Fit2D of the marcasite sample reacted at pH~12.
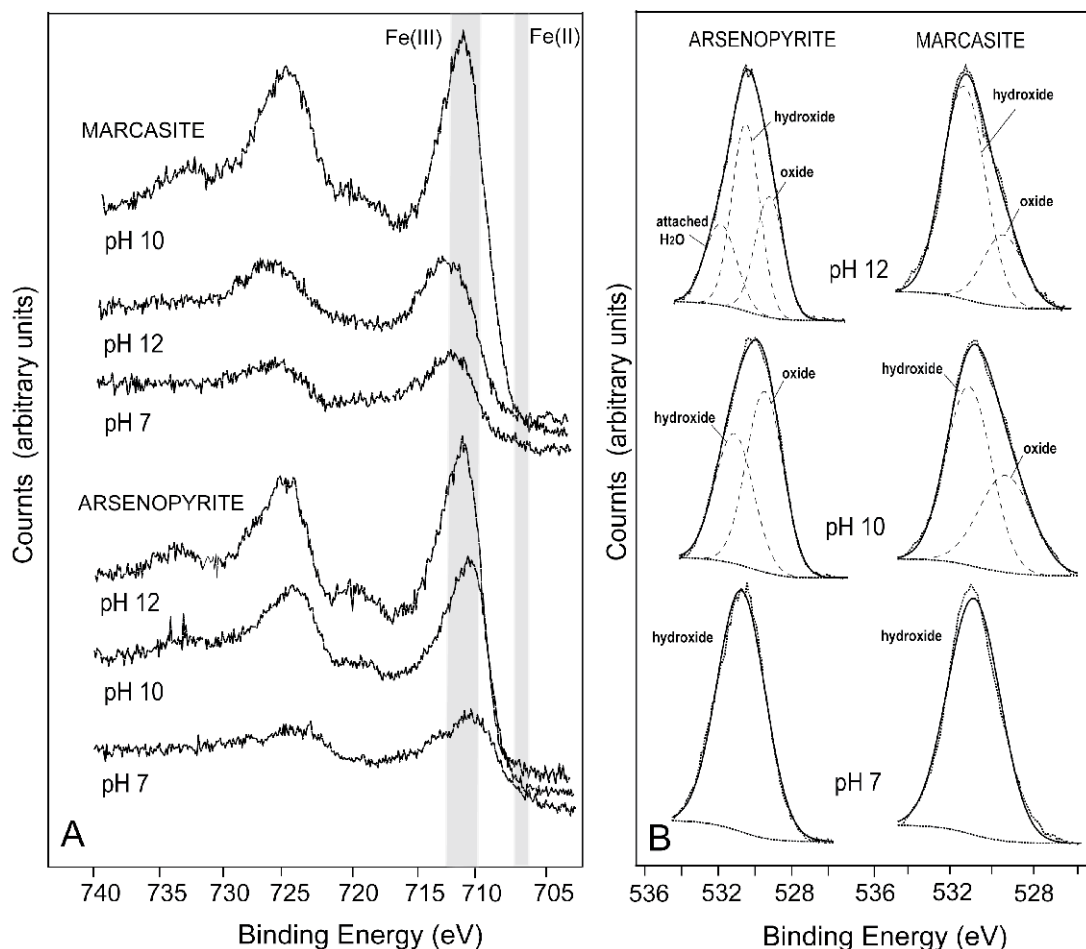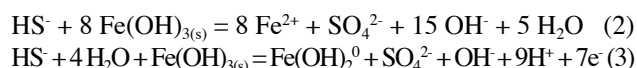
FIGURE 5 | XPS A) Fe 2p$_{3/2}$ and B) O1s spectra of arsenopyrite and marcasite samples reacted.

pH 7 each species represent around the 50% of the total sulphur and at pH 10 the sulphates increase up to 75%. The absence of Fe(II)-S peaks in the Fe 2p spectra (at 707eV), indicates that pristine marcasite surface is not exposed. However, S2p spectra reveal the presence of the reduced sulphur signal 162.8eV corresponding to the disulphide region (S$_2^{2-}$ of FeS$_2$).

Since Fe(II) is absent from the Fe2p spectra of Figure 6A, these reduced sulphur species may be bonded to Fe(III) as observed for oxidized pyrrhotite, pyrite and arsenopyrite surfaces (Mycroft *et al.*, 1990; Pratt *et al.*, 1994; Nesbitt and Muir, 1998). At pH 12 these reduced species are not observed and sulphates represent the 80% of the total sulphur and polysulphides represent the 20%.

The coexistence of the S(-II) species with the Fe(III) at pH 7 and 10 could be explained by the slow kinetics of the oxidation reaction of H$_2$S by Fe(III) (eq. 2), which is 4 and 6 orders of magnitude slower than those of S(-II) and Fe(II) oxidation by O$_2$, respectively (Canavan *et al.*, 2006; Couture *et al.*, 2010). However, S(-II) species

are not present in the samples reacted at pH 12, which could be accounted for the fact that this reaction is faster at pH>10.3, due to the change in the speciation of Fe(II) (eq. 3).

$$HS^- + 8\,Fe(OH)_{3(s)} = 8\,Fe^{2+} + SO_4^{2-} + 15\,OH^- + 5\,H_2O \quad (2)$$
$$HS^- + 4\,H_2O + Fe(OH)_{3(s)} = Fe(OH)_2^0 + SO_4^{2-} + OH^- + 9\,H^+ + 7\,e^- \quad (3)$$

These results indicate that during the reaction of marcasite under neutral to alkaline conditions disulphides are oxidized to polysulphides, which are oxidized to sulphates in the surface.

The arsenopyrite spectra show a major peak at pH 7, 10 and 12 corresponding to polysulphides and that represents the 100% and up the 80% and 70% of the total sulphur, respectively. The results suggest that the polysulphides are oxidized to sulphates during the reaction. As in the case of marcasite, the absence of the Fe(II)-S peaks and the presence of reduced signals (polysulphides) could indicate that they could be within or beneath the Fe precipitates.
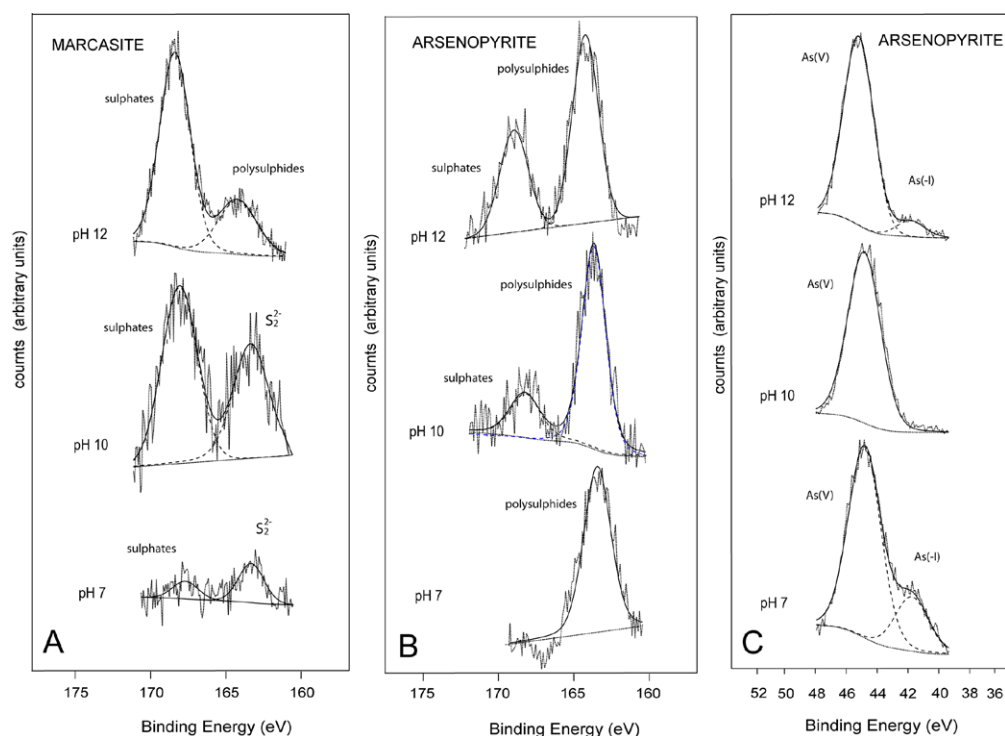
FIGURE 6 | Fitted S2p spectra of marcasite and arsenopyrite and As3d spectra of arsenopyrite representative samples reacted at pH 7.2-7.5, 10.0-10.5 and 12.3-12.6.

In both minerals, as the pH increased the peak at 168-169eV associated to the sulphates strongly increased in the S2p spectra indicating that the sulphate formed during the sulphides dissolution is accumulating in the mineral surface. The formation of sulphur-oxy species at alkaline pH values, particularly sulphate together with ferric oxide/hydroxide in the surface layers, has been identified in different XPS studies of sulphides (Brion, 1980; Buckley and Woods, 1987; Richardson and Vaughan, 1989). For example, sulphate species have been observed in pyrite surfaces after being exposed to alkaline solutions (Buckley and Woods 1985a,b; 1987). Similarly pyrrhotite surfaces after reacting with alkaline solutions resulted in ferric hydroxide, sulphate species and iron-deficient sulphide. According to Smart *et al.* (1998) after the reaction of the iron containing sulphides with neutral or alkaline solutions, the Fe(III) oxidized species remain on the surface together with sulphides and polysulphide species and after prolonged periods in solution, all surfaces show the formation of sulphate ions.

As3d spectra

The examination of As3d peaks of arsenopyrite (Fig. 6C) shows a major peak at approximately 44.8-45.2eV, which corresponds to As(V) (Nesbitt and Muir, 1998). The shoulder of the low binding energy side may indicate the contribution of As(-I) species at binding energy of 41.8eV (Buckley and Walker, 1988; Nesbitt *et al.*, 1995). The contribution of this reduced species (As(-I)) is more significant in the sample reacted at pH 7 (23%), whereas at pH 10 is not representative and at pH 12 is lower than the 10% of the sulphur species, suggesting that As in the arsenopyrite surface is mostly in its As(V) oxidized form. The presence of these additional reduced species (As(-I)) together with the absence of Fe(II) in the Fe 2p spectra could indicate, as in the case of the reduced suphur species, that As(-I) could be bonded to Fe(III) in the arsenopyrite surface mainly when the reaction takes place at pH 7.

Surface stoichiometry

XPS analysis conducted on the oxidized marcasite and arsenopyrite confirmed an enrichment of iron in the surface in all the experiments with respect to the initial samples (Table 2). Iron is accumulated over the sulphide surface, as previously reported, as iron oxide and hydroxide phases such as ferrihydrite, goethite, hematite, maghemite or lepidocrocite (Nicholson *et al.*, 1990; Koslides and Ciminelli, 1992; Hiskey and Sanchez, 1995, Pérez-López *et al.*, 2007). In addition, an enrichment in arsenic has been also observed on the arsenopyrite surface of the reacted samples at pH 9.8 and 12.4. This excess of arsenic could have been sorbed or precipitated as a new phase, which is in agreement with the fact that arsenic concentrations were stoichiometrically lower than sulphur in the output solution.

Sample	S	Fe	As	S:Fe	As:S	Fe:As	pH
		(at %)*					
MRC Initial **	67	33	-	2.0	-	-	-
MRC-1	25	75	-	0.3	-	-	7.4
MRC-2	43	57	-	0.8	-	-	7.6
MRC-3	33	67	-	0.5	-	-	9.1
MRC-4	38	62	-	0.6	-	-	8.9
MRC-5	13	87	-	0.2	-	-	9.9
MRC-6	31	69	-	0.5	-	-	9.7
MRC-7	34	66	-	0.5	-	-	12.6
MRC-8	32	68	-	0.5	-	-	12.6
Aspy Initial **	34	33	32	1.0	1.0	1.0	-
ASP-1	34	47	19	0.7	0.6	1.4	9.1
ASP-2	15	47	36	0.3	2.4	3.2	9.8
ASP-3	14	62	22	0.2	1.6	4.4	12.4

* Estimated normalized out the rest of elements (oxygen and adventitious carbon)

** Based on electron microprobe analysis

Brunauer, Emmett and Teller surface area

Brunauer, Emmett and Teller (BET) area after the reaction showed a significant increase in arsenopyrite and marcasite with initial values of 0.6 and $0.9m^2/g$ and maximum values of 3.5 to $5.2m^2/g$ after the experiments. This enhancement of specific surface area could be due to the fact that the poorly crystalline precipitates of new Fe-bearing phases on arsenopyrite and marcasite surfaces originate large surface areas (Meng and Letterman, 1993a,b), and thus an increase in the surface area of the final product.

S K-edge X-ray absorption near edge structure

Figure 7A shows the µXANES spectra of two reference minerals used to define the position and the features associated with S_2^{2-} and S^{6+} sulphur species. These spectra were taken from the ID21 sulphur XANES spectra database. For the reduced sulphur species, pyrite was used as reference material. Pyrite is characterized by a main peak at 2472.1eV which was used as the criterion to establish the presence of inorganic disulphide in the samples analyzed (Prietzel *et al.*, 2003). In the case of the oxidized sulphur, a gypsum spectrum has been used and, as observed, sulphate is characterized by a sharp peak at 2482.8eV. Those peak assignments are consistent with previous works on S speciation by XANES (Huffman *et al.*, 1991; Xia *et al.*, 1998; Prietzel *et al.*, 2007).

Figure 7B shows the average of the normalized µXANES spectra at the S K-edge of the bulk samples of arsenopyrite reacted at pH 7.5 and 9. The spectra show, in all samples, the characteristic broad peak at 2472.1eV observed in pyrite indicating the predominance of disulphide in the samples. In addition, the samples that reacted at pH 9 show a small shoulder at 2482.5eV that is consistent with minor amounts of sulphate in the sample. Therefore, the results indicate a variation in sulphur species with pH and an increase of the sulphate content as pH increased which is in good agreement with the XPS results (see Fig. 6).
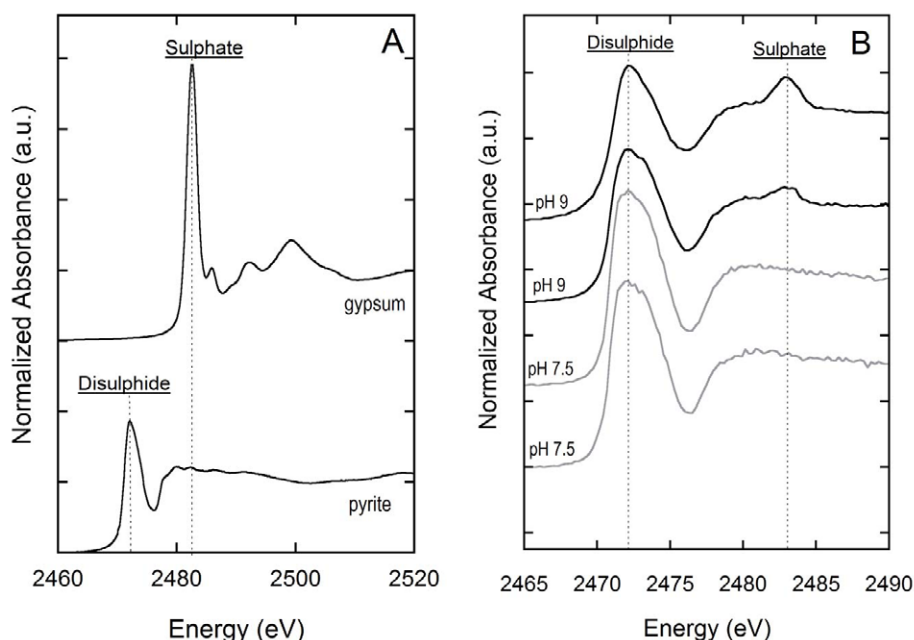

FIGURE 7 | A) Sulphur µXANES spectra used to define the peak positions for sulphide (S2-) and sulphate (S6+) species. Both spectra were taken from the ID21 database. The vertical lines indicate the energy of the main peaks: 2472.3eV that corresponds to sulphide peak and 2482.8eV for the sulphate peak. B) Sulphur µXANES spectra of the bulk samples of arsenopyrite reacted at pH 7.5 and 9.1.
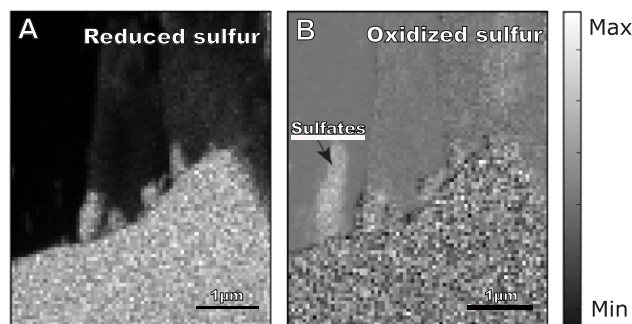
FIGURE 8 | Normalized images of the distribution of A) reduced sulfur and B) oxidized sulphur in the marcasite sample reacted at pH 12.4. Map size: 13.2 x 5.2 µm2.

Owing to the fact that the samples that reacted at higher pH showed higher sulphate concentrations, two samples of marcasite and arsenopyrite that reacted at pH 9 were examined by µXANES at the S K-edge. However, despite the presence of small quantities of sulphate in the S K-edge of the bulk arsenopyrite samples (Fig. 7B) no sulphate was observed in the analyses of different points of these samples, suggesting that the sulphate is in a very low concentration and furthermore it could be heterogeneously distributed. Therefore, considering those results, the sample of marcasite that reacted at the highest pH studied (pH = 12) was selected to study the distribution of sulphate vs. disulphide in the grains and mainly in the secondary Fe precipitates formed in the boundaries during the mineral dissolution. To map the distribution of oxidized and reduced states of sulphur in the sample the method applied by (Cotte *et al*., 2006). The XRF intensity was measured at three different energies: i) at 2472.1eV to favour the excitation of reduced sulphurs; ii) at 2482.8eV to favour the excitation of oxidized sulphurs; and iii) at 2500eV to measure the global XRF of sulphur, whatever its speciation. The map obtained at 2472.1eV corresponds to the most reduced sulphur (Fig. 8A) and the one acquired at 2500eV shows all sulphur. Therefore, the subtraction of the map at 2482.8eV from the one obtained at 2500eV shows primarily the oxidized sulphur in the sample (Fig. 8B). The results showed that sulphates are mainly located in the border of the grain. In addition, µXANES spectra of different points from an area inside a grain to the border of the grain were performed (Fig. 9). It is clearly observed a variation in the sulphur oxidation state in the sample, being the sulphates concentrated towards the border of the grain. Points 1 to 3 were obtained inside the marcasite grain, which correspond to the area with the highest reduced sulphur signal intensity, and they perfectly fit with the disulphide feature with a peak at 2472.1eV and with little or no detectable sulphate. However, points 4, 5 and 6, obtained in the layer that covers the grain, showed a peak at 2482.5eV corresponding to sulphates. The relative intensity of the sulphate peak is higher in the points 5 and 6 located out of the marcasite grain.

As stated in the S2p spectra section, the presence of sulphur oxy species as sulphate on the sulphide surfaces after reacting with alkaline solutions has been previously reported in sulphide studies (*e.g*., pyrite, chalcopyrite, pentlandite). However, it is worth noting that the role of sulphate species in passivation of oxidation is still on contention when comparing to the role of hydroxides, oxyhydroxides and oxides (Smart *et al*., 1998).

Fe K-edge X-ray absorption near edge structure

The spatial variation in the iron oxidation state of the selected sample of arsenopyrite that reacted at pH 9 was studied by analyzing different spots of the sample (Fig. 10A). The normalized µXANES spectra and corresponding first-derivative for the different spots along
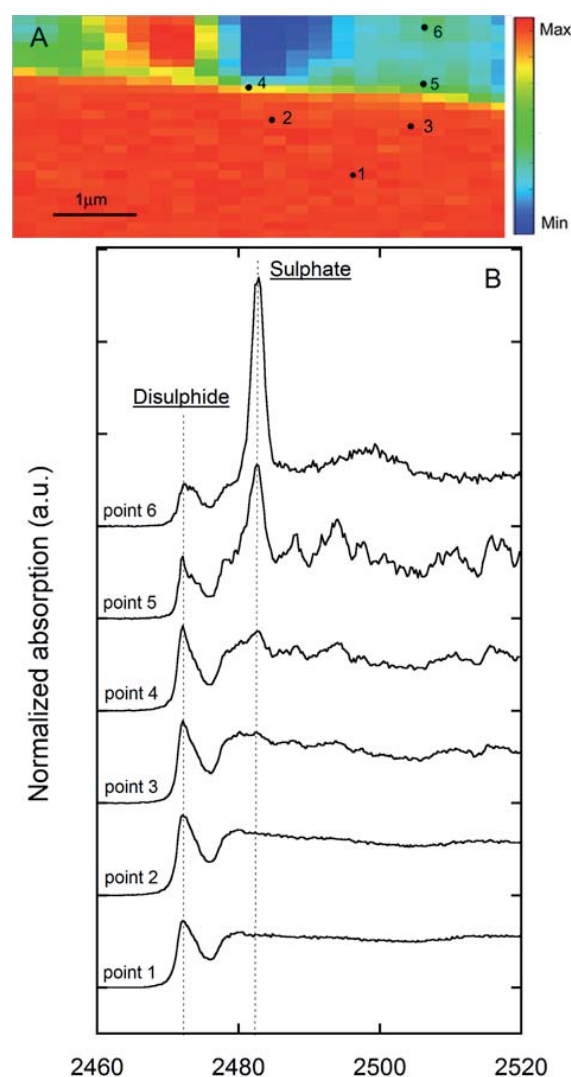

FIGURE 9 | A) Marcasite fluorescence map (size 13.2 x 5.2µm²) obtained at 2482.8eV. Red color correspond to the areas more concentrated in sulphur, whereas blue correspond to the less sulphur concentrated areas; B) X-ray absorption spectra at the S K-edge obtained at different points of the fluorescence map.
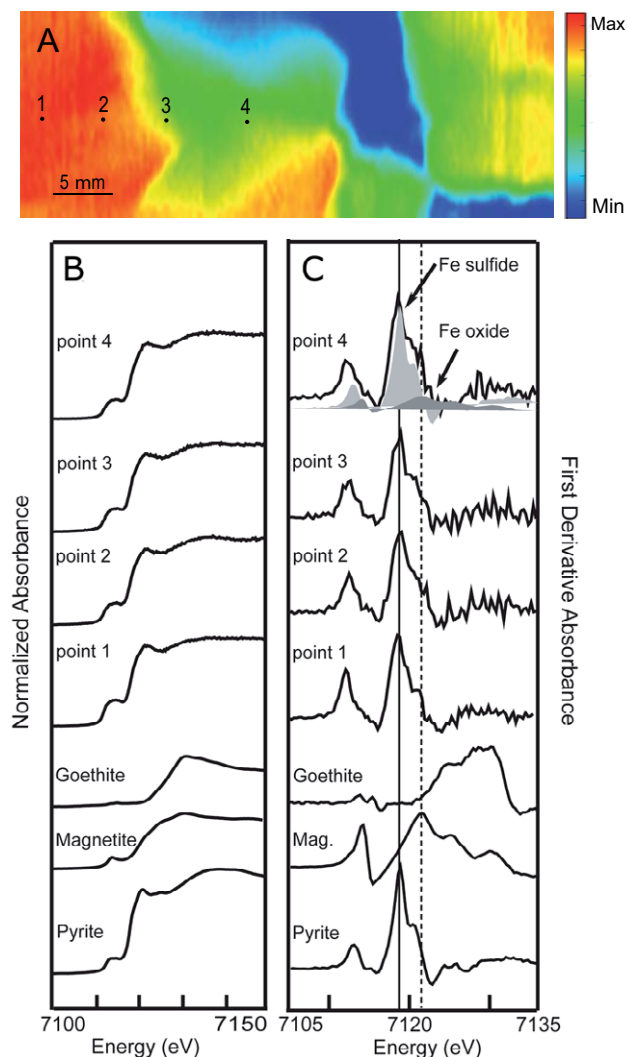
FIGURE 10 A) Iron fluorescence map of the arsenopyrite reacted at pH 9 obtained at 7200eV; map size: 18.2 x 30.2µm²; B) Iron K-edge µXANES; C) corresponding first-derivative spectra compared to reference spectra. Shading in the first-derivative spectra of point 4 shows the fraction of iron associated mainly to a sulphide phase (pyrite) and a minor Fe oxide phase (magnetite) after performing linear combination fit with Athena.

the sample and three reference compounds are shown in Figure 10B. All the Fe µXANES spectra of the reacted sample are clearly different from the Fe oxides and more similar to the Fe sulphide model compound shown (pyrite). The normalized first derivative of iron µXANES of the reacted sample shows a peak inflection at pre-edge 7112.0-7112.3eV, a primary peak inflection at 7118.3-7118.5eV and a small peak at 7130eV. These main derivative peaks correspond to those assigned to Fe in sulphides (*e.g.* O'Day *et al.*, 2004). The presence of a small shoulder at higher energies could suggest the presence of an Fe oxide component which would increase toward the border of the grain (Fig. 10B, point 4). Fits for the XANES spectra over the Fe-region for reacted samples were linear combinations of Fe-reference standards. After considering different Fe-

compounds (*e.g.* goethite, ferrihydrite, hematite) the results showed that magnetite could contribute to the spectra but in low percentages (Fig. 10C, point 4).

In addition to the study of the normalized Fe µXANES spectra and corresponding first derivative, the pre-edge features in the Fe µXANES spectra have been analyzed. As previously reported, the comparison of the pre-edge features of model compounds and reacted samples may provide insight into the oxidation state of the samples (Wilke *et al.*, 2001, 2009; Berry *et al.*, 2003; Métrich *et al.*, 2006). The Fe-K pre-edge features were extracted from the normalized spectra by selecting the 7105-7120eV region. A spline function was then used to extract the pre-edge feature defining a smooth curve through the absorption edge using the data several eV before and after the pre-edge feature as used in previous studies (Wilke *et al.*, 2001; Berry *et al.*, 2003). The pre-edge extracted from the spectra of two model compounds (pyrite as representative of Fe^{2+} and ferrihydrite of Fe^{3+}) and the reacted sample (points showed in Fig. 10) are presented in Figure 11. As reported in previous studies (*e.g.* Métrich *et al.*, 2006), the pre-edge shows a shift to higher energies with increasing the $Fe^{3+}/\Sigma Fe$ ratio. The results suggest that there is a mixture of Fe^{2+} and Fe^{3+} in the studied points but with a predominance of Fe^{2+}. In addition, the small shift observed when comparing the spectra from the center of the grain to the spectra from the border may indicate an increase in ferric iron in the border.

Technical restrictions

The spectroscopic techniques used in this study have provided information about the nature of the surface products formed by the interaction of arsenopyrite and marcasite with neutral and alkaline solutions. The different techniques used provide different information of the samples. Whereas the analysis depth of XPS is limited to the first 5-10 nanometers, µXANES depth generally is
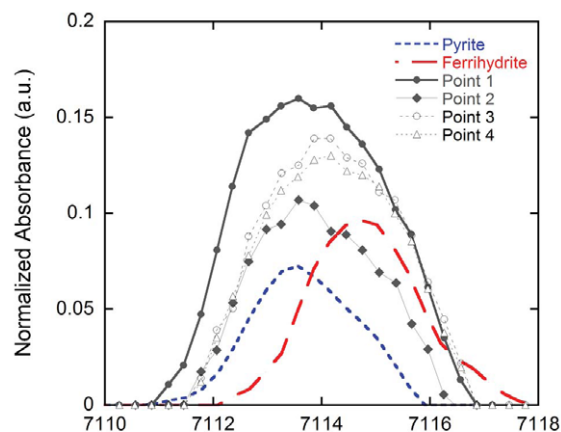

FIGURE 11 Normalized pre-edge spectra (Fe-K-edge) of model compounds and different µXANES spectra of the arsenopyrite sample reacted at pH 9.

in the order of tens of microns and XRD measurements were done in transmission mode analyzing all the sample thickness. Specifically, the depth of penetration of the incident X-radiation in marcasite and arsenopyrite at the iron energy (7200eV) is around 7.5-8μm but decreases at the energy of lighter elements such as sulphur (2500eV of incident X-radiation) to a penetration of depth of around 1.1-1.2μm. Thus, the first technique should reveal more detailed information on the surface layer composition whereas the XANES and XRD provide more information about the bulk composition of the minerals under investigation. Comparing the XPS and XANES spectra, some compositional differences are observed. These differences could be due to the limitations of those techniques in the determination of some species in low concentrations. For example, the presence of some sulphur species such as polysulphides and disulphides is observed by XPS but not by μXANES; this could be due to the fact that sulphides (mono-, di-, and polysulphides) are rarely distinguished using S K-edge XANES (Morra *et al.*, 1997; Xia *et al.*, 1998; Hutchinson *et al.*, 2001). In addition, the presence of ferric iron is more evident in the XPS and XRD results in comparison to those of μXANES.

CONCLUSIONS

Marcasite and arsenopyrite oxidizes under neutral to alkaline conditions to form surface coatings preventing the oxidation of these sulphides. The presence of iron minerals in these coatings, neoformed during the marcasite and arsenopyrite dissolution process, have been confirmed by the decrease of iron concentration in the output solution of the flow through experiments together with the analysis of the surfaces by means of microscopic, spectroscopic and synchrotron techniques. The thermodynamic models predict the precipitation of iron oxides which was confirmed experimentally by the micro-X-ray diffraction results by the presence of goethite (α-FeOOH) when the reaction occurs at pH 12. At lower pH values than 12 the coating products seem to be poorly crystalline. In addition, the XPS analysis of the surface coatings corroborated that the coatings are mainly composed of iron oxides and iron hydroxides and also showed the presence of sulphur species (polysulphides and sulphates) in minor concentration. These surface products vary with pH with an increase of the sulphate content in the surface layer with the increase of pH. Furthermore, the μXANES results suggest that sulphates increased their concentrations from the grain, mainly composed by disulphide, to the grain boundary. In the same way ferric iron seemed to increase to the border of the grain.

Therefore, considering our results, we can conclude that the dissolution of marcasite and arsenopyrite under neutral to alkaline conditions led to the formation of precipitates of micrometer-scale, which were observed by SEM and μXANES. These oxidation products, which remain in a thin surface layer over the sulphide grains, are composed of ferric iron oxide/hydroxide and sulphur oxidized species (mainly sulfates) showing a different composition to the coated sulphide.

REFERENCES

Acero, P., Cama, J., Ayora, C., Asta, M.P., 2009. Chalcopyrite dissolution rate law from pH 1 to 3. Geologica Acta, 7(3), 389-397.

Allison, J.D., Brown, D.S., Novo-Gradac, K.J. 1990. MINTEQA2/PRODEFA2, a geochemical assessment model for environmental systems: Version 3.0. Office of Research and Development, US Environmental Protection Agency, Athens (USA).

Asta, M.P., Cama, J., Soler, J.M., Arvidson, R.S., Lütge, A., 2008. Interferometric study of pyrite surface reactivity in acidic conditions. American Mineralogist, 93, 508-519.

Asta, M.P., Cama, J., Acero, P., 2010a. Dissolution kinetics of marcasite at acidic pH. European Journal of Mineralogy, 22, 49-61.

Asta, M.P., Cama, J., Ayora, C., Acero, P., de Giudici, G., 2010b. Arsenopyrite dissolution rates in O_2-bearing solutions. Chemical Geology, 273, 272-285.

Ball, J.W., Nordstrom, D.K., 2001. User's manual for WATEQ4F with revised thermodynamic database and test cases for calculating speciation of major, trace and redox elements

in natural waters (Revised and reprinted, April, 2001). U.S. Geological Survey Water-Resources Investigation Report, 91-183, 188pp.

Belzile, N., Chen, Y.W., Cai, M.F., Li, Y., 2004. A review on pyrrhotite oxidation. Journal of Geochemical Exploration, 84, 65-76.

Beattie, M.J.V., Poling, G.W., 1987. A study of the surface oxidation of arsenopyrite using cyclic voltammetry. International Journal of Mineral Processing, 20, 87-108.

Berry, A.J., O'Neil, H.ST.C., Jayasuriya, K.D., Campbell, S.J., Foran, G.J., 2003. XANES calibrations for the oxidation state of iron in a silicate glass. American Mineralogist, 88, 963-977.

Bhakta, P., Langhans, J.W., Lei, K.P.V., 1989. Alkaline oxidative leaching of gold-bearing arsenopyrite ores. U.S. Department of Interior, Bureau of Mines, RI 9258, 16pp.

Bonnissel-Gissinger, P., Alnot, M., Ehrhardt, J.J., Behra, P., 1998. Surface oxidation of pyrite as a function of pH. Environmental Science and Technology, 32, 2839-2845.

Briggs, D., Seah M.P., 1990. Practical surface analysis. Volume 1. Auger and X-ray photoelectron spectroscopy. John Wiley and Sons, 2nd edition, 657pp.

Brion, D., 1980. Etude par spectroscopie de photoelectrons de la degradation superficielle de FeS_2, ZnS et PbS a l'air et dans l'eau. (Photoelectron spectroscopic study of the surface degradation of FeS_2, ZnS and PbS in air and water). Applied Surface Science, 5, 133-152.

Buckley, A.N., 1987. The surface oxidation of pyrite. Applied Surface Science, 27, 347-452.

Buckley, A.N., Woods, R., 1984. An X-ray photoelectron spectroscopic study of the oxidation of chalcopyrite. Australian Journal of Chemistry, 37, 2403-2413.

Buckley, A.N., Woods, R., 1985a. X-ray photoelectron spectroscopy of oxidized pyrrhotite surfaces. I Exposure to air. Applied Surface Science, 22-23, 280-287.

Buckley, A.N., Woods, R., 1985b. X-ray photoelectron spectroscopy of oxidized pyrrhotite surfaces. I. Exposure to aqueous solutions. Applied Surface Science, 20, 472-480.

Buckley, A.N., Woods, R., 1987. The surface oxidation of pyrite. Applied Surface Science, 27, 437-452.

Buckley, A.N., Walker, G.W., 1988. The surface-composition of arsenopyrite exposed to oxidizing environments. Applied Surface Science, 35, 227-240.

Caldeira, C.L., Ciminelli, V.S.T., Dias, A., Osseo-Asare, K., 2003. Pyrite oxidation in alkaline solutions: nature of the product layer. International Journal of Mineral Processing, 72, 373-386.

Canavan, R., Slomp, C., Jourabchi, P., Van Cappellen, P., Laverman, A., Van den Berg, G., 2006. Organic matter mineralization in sediment of a coastal freshwater lake and response to salinization. Geochimica et Cosmochimica Acta, 70, 2836-2855.

Cornell, R.M., Schwertmann, U., 1996. The iron oxides. New York, Wiley-VCH, 573pp.

Cotte, M., Susini, J., Metrich, N., Moscato, A., Gratziu, C., Bertagnini, A., Pagano, M., 2006. Blackening of Pompeian cinnabar paintings: X-ray microspectroscopy analysis. Analytical Chemistry, 78, 7484-7492.

Cotte, M., Susini, J., Solé, V., Taniguchi, Y., Chillida, J., Checroun, E., Walter, P., 2008. Applications of synchrotron-based micro-imaging techniques to the chemical analysis of ancient paintings. Journal of Analytical Atomic Spectrometry, 23, 820-828.

Couture, R.-M., Shafei, B., Van Cappellen, P., Tessier, A., Gobeil, C. 2010. Non-steady state modeling of arsenic diagenesis in lake sediments. Environmental Science and Technology, 44, 197-203.

Elsetinow, A.R., Strongin, D.R., Borda, M.J., Schoonen, M.A., Rosso, K.M., 2003. Characterization of the structure and the surface reactivity of a marcasite thin film. Geochimica et Cosmochimica Acta, 67, 807-812.

Evangelou, V.P., 1995. Pyrite oxidation and Its control. Boca Raton (USA), CRC Press, 285pp.

Evangelou, V.P., 1996. Pyrite oxidation inhibition in coal waste by PO_4 and H_2O_2 pH buffered pretreatment. International Journal of Surface Mining, Reclamation and Environment, 10, 135-142.

Evangelou, V.P., 2001. Pyrite microencapsulation technologies: principles and potential field application. Ecological Engineering, 17, 165-178.

Evangelou, V.P., Seta, A.K., Holt, A., 1998. Potential role of bicarbonate during pyrite oxidation. Environmental Science and Technology, 32, 2084-2091.

Ferris, F.G., Tazaki, K., Fyfe, W.S., 1989. Iron oxides in acid mine drainage environments and their association with bacteria. Chemical Geology, 74, 321-330.

Fytas, K., Evangelou, B., 1998. Phosphate coating on pyrite to prevent acid mine drainage. International Journal of Mining, Reclamation and Environment, 12, 101-104.

Fytas, K., Evangelou, B., 1999. Application of silicate coatings on pyrite to prevent acid mine drainage. Proceedings, Mining and the Environment II, Sudbury, Ontario, 3, 1199-1207.

Fytas, K., Bousquet, P., 2002. Silicate micro-encapsulation of pyrite to prevent acid mine drainage. The Canadian Institute of Mining, Metallurgy and Petroleum Bulletin, 95(1063), 96-99.

Johnson, D.B., Hallberg, K.B., 2005. Acid mine drainage remediation options: a review. Science of the Total Environment, 338, 3-14.

Hacquard, E., Bessiere, J., Alnot, M., Ehrhardt, J.J., 1999. Surface spectroscopic study of the adsorption of Ni(II) on pyrite and arsenopyrite at pH 10. Surface and Interface Analysis, 27, 849-860.

Hammersley, A.P., Svensson, S.O., Han, M., Fitch, A.N., Hausermann, D., 1996. Two dimensional detector software: from real detector to idealised image or two-theta scan. High Pressure Research, 14, 235-248.

Harmer, S.L., Nesbitt, H.W., 2004. Stabilization of pyrite (FeS_2),marcasite (FeS_2), arsenopyrite (FeAsS) and loellingite (FeAS2) surfaces by polymerization and auto-redox reactions. Surface Science, 564, 38-52.

Harvey, D.T., Linton, R.W., 1981. Chemical characterization of hydrous ferrie oxides by X-ray photoelectron spectroscopy. Analytical Chemistry, 53,1648-1688.

Hiskey, J.B., Sanchez, V.M., 1995. Alkaline pressure oxidation of a gold-bearing arsenopyrite concentrate. Mineral Processing and Extractive Metallurgy Review, 15, 61-74.

Hood, Y.A., 1991. The kinetics of pyrite oxidation in marine systems. Ph.D. Thesis. University of Miami (USA), 223pp.

Huang, X., Evangelou, V.P., 1993. Suppression of Pyrite Oxidation Rate by Phosphate Addition, Environmental Geochemistry of Sulfide Oxidation. American Chemical Society (ACS) Symposium Series, American Chemical Society, 550, 562-573.

Huffman, G.P., Mitra, S., Huggins, F.E., Shah, N., Vaidya, S., Lu, F., 1991. Quantitative analysis of all major forms of sulfur in coal by x-ray absorption fine structure spectroscopy. Energy Fuels, 5, 574-581.

Huminicki, D.M.C., Rimstidt, J.D., 2009. Iron oxyhydroxide coating of pyrite for acid mine drainage control. Applied Geochemistry, 24, 1626-1634.

Hutchison, K.J., Hesterberg, D., Chou, J.W. 2001. Stability of reduced organic sulfur in humic acid as affected by aeration and pH. Soil Science Society of America Journal, 65, 704-709.

Jurjovec, J., Ptacek, C.J., Blowes, D.W., 2002. Acid neutralization mechanisms and metal reslease in mine tailings: A laboratory column experiment. Gechimica et Cosmochimica Acta, 66, 1511-1523.

Koslides, T., Ciminelli, V.S.T., 1992. Pressure oxidation of arsenopyrite and pyrite in alkaline-solutions. Hydrometallurgy, 30, 87-106.

Lasaga, A.C., 1998. Kinetic Theory in the Earth Sciences. Princeton University Press, 728pp.

Mathews, C.T., Robins, R.G., 1972. The oxidation of ferrous disulphide by ferric sulphate. Australian Chemical Engineering, 13, 21-25.

Mathews, C.T., Robins, R.G., 1974. Oxidation of iron disulphide by molecular oxygen. Australian Chemical Engineering, 15, 19-24.

McIntyre, N.S., Zeratuk, D.G., 1977. X-ray photoelectron spectroscopic studies of iron oxides. Analytical Chemistry, 49, 1521-1529.

McKibben, M.A., Tallant, B.A., del Angel, J.K., 2008. Kinetics of inorganic arsenopyrite oxidation in acidic aqueous solutions. Applied Geochemistry, 23, 121-135.

Meng, X., Letterman, R.D., 1993a. Modeling ion adsorption on aluminum hydroxide-modified silica. Environmental Science and Technology, 27, 1924-1929.

Meng, X., Letterman, R.D., 1993b. Effect of component oxide interaction on the adsorption properties of mixed oxides. Environmental Science and Technology, 27, 970-975.

Métrich, N., Susini, J., Foy, E., Farges, F., Massare, D., Sylla, L., Lequien, S., Bonnin-Mosbah, M., 2006. Redox state of iron in peralkaline rhyolitic glass/melt: X-ray absorption micro-spectroscopy experiments at high temperature. Chemical Geology, 231, 350-362.

Mikhlin, Y.L., Romanchenko, A.S., Asanov, I.P., 2006. Oxidation of arsenopyrite and deposition of gold on the oxidized surfaces: A scanning probe microscopy, tunneling spectroscopy and XPS study. Geochimica Cosmochimica Acta, 70, 4874-4888.

Morra, M.J., Fendorf, S.E., Brown, P.D., 1997. Speciation of sulfur in humic and fulvic acids using X-ray absorption near-edge structure (XANES) spectroscopy. Gechimica et Cosmochimica Acta, 3, 683-688.

Mycroft, J.R., Bancroft, G.M., McIntyre, N.S., Lorimer, J.W., Hill, I.R., 1990. Detection of Sulphur and polysulphides on electrochemically oxidized pyrite surfaces by X-ray photoelectron-spectroscopy and Raman spectroscopy. Journal of Electroanalytical Chemistry, 292, 139-152.

Mylona, E., Xenidis, A., Paspaliaris, I., 2000. Inhibition of acid generation from sulphidic wastes by the addition of small amounts of limestone. Minerals Engineering, 13, 1161-1175.

Nesbitt, H.W., Muir, I.J., 1994. X-ray photoelectron spectroscopic study of a pristine pyrite surface reacted with water-vapor and air. Geochimica et Cosmochimica Acta, 58, 4667-4679.

Nesbitt, H.W., Muir, I.J., 1998. Oxidation states and speciation of secondary products on pyrite and arsenopyrite reacted with mine waste waters and air. Mineralogy and Petrology, 62, 123-144.

Nesbitt, H.W., Muir, I.J., Pratt, A.R., 1995. Oxidation of arsenopyrite by air and air-saturated, distilled water, and implications for mechanism of oxidation. Geochimica et Cosmochimica Acta, 59, 1773-1786.

Nicholson, R.V., Gilham, R.V., Reardon, E.J., 1988. Pyrite oxidation in carbonate-buffered solutions 1: experimental kinetics. Geochimica et Cosmochimica Acta, 52, 1077-1085.

Nicholson, R.V., Gilham, R.V., Reardon, E.J., 1990. Pyrite oxidation in carbonate-buffered solutions: 2. rate control by oxide coatings. Geochimica et Cosmochimica Acta, 54, 395-402.

Nordstrom, D.K., Alpers, C.N., 1999. Negative pH, efflorescent mineralogy, and consequences for environmental restoration at the Iron Mountain Superfund site, California. United States of America, Proceedings of the National Academy of Sciences, 96, 3455-3462.

Nyavor, K., Egiebor, N.O., 1995. Control of pyrite oxidation by phosphate coating. Science of the Total Environment, 162, 225-237.

O'Day, P.A., Rivera, N.Jr., Root, R., Carrol, S.A., 2004. X-ray absorption spectroscopic study of Fe reference compounds for the analysis of natural sediments. American Mineralogist, 89, 572-585.

Parkhurst, D.L., Appelo, C.A.J., 1999. User's Guide to PHREEQC (Version 2), a computer program for speciation, batch reaction, one-dimensional transport, and inverse geochemical calculations. Water Resources Research, Inverstigations Report, 99-4259, 312pp.

Pérez-López, R., Cama, J., Nieto, J.M., Ayora, C., 2007. The iron-coating role on the oxidation kinetics of a pyritic sludge doped with fly ash. Geochimica et Cosmochimica Acta, 71, 1921-1934.

Pratt, A.R., Nesbitt, H.W., Muir, I.J., 1994. Generation of acids from mine waste - oxidative leaching of pyrrhotite in dilute H_2SO_4 solutions at pH 3.0. Geochimica et Cosmochimica Acta, 58, 5147-5159.

Pratt, A.R., McIntyre, N.S., Splinter, S.J., 1998. Deconvolution of pyrite marcasite and arsenopyrite XPS spectra using the maximum entropy method. Surface Science, 396, 266-272.

Prietzel, J., Thieme, J., Neuhäusker, U., Susini, J., Kögel-Knabner, I., 2003. Speciation of sulphur in soils and soil particles by X-ray spectromicroscopy. European Journal of Soil Science, 54, 423-433.

Prietzel, J., Thieme, J., Salomé, M., Knicker, H., 2007. Sulfur K-edge XANES spectroscopy reveals differences in sulfur speciation of bulk soils, humic acid, fulvic acid, and particle size separates. Soil Biology and Biochemistry, 39, 877-890.

Ravel, B., Newville, M.J., 2005. ATHENA, ARTEMIS, HEPHAESTUS: data analysis for X-ray absorption spectroscopy using IFEFFIT. Synchrotron Radiation, 12, 537-541.

Richardson, S., Vaughan, D.J., 1989. Arsenopyrite - a spectroscopic investigation of altered surfaces. Mineralogical Magazine, 53, 223-229.

Rinker, M.J., Nesbitt, H.W., Pratt, A.R., 1997. Marcasite oxidation in low-temperature acidic (pH 3.0) solutions: Mechanism and rate laws. American Mineralogist, 82, 900-912.

Scheidegger, A., Borkovek, M., Sticher, H., 1993. Coating of silica sand with goethite: preparation and analytical identification. Geoderma, 58, 43-66.

Singer, P.C., Stumm, W., 1970. Acidic mine drainage: the rate-limiting step. Science, 167, 1121-1123.

Solé, V.A., Papillon, E., Cotte, M., Walter, Ph., Susino, J., 2007. A multiplatform code for the analysis of energy-dispersive X-ray fluorescence spectra. Spectrochimica Acta, Part B, Atomic Spectroscopy, 62, 63-68.

Smart, R.St.C., Amarantidis, J., Skinner, W., Prestidge, C.A., La Vanier, L., Grano, S., 1998. Surface analytical studies of oxidation and collector adsorption in sulfide mineral flotation. Scanning Microscopy, 12, 553-583.

Somogyi, A., Drakopoulos, M., Vincze, L., Vekemans, B., Camerani, C., Janssens, K., Snigirev, A., Adams, F., 2001. ID18F: a new micro- X-ray fluorescence end-station at the European Synchrotron Radiation Facility (ESRF): preliminary results. X-Ray Spectrometry, 30, 242-252.

Uhlig, I., Szargan, R., Nesbitt, H.W., Laajalehto, K., 2001. Surface states and reactivity of pyrite and marcasite. Applied Surface Science, 179, 222-229.

Vandiviere, M.M., Evangelou, V.P., 1998. Comparative testing between conventional and microencapsulation approaches in controlling pyrite oxidation. Journal of Geochemical Exploration, 64, 161-176.

Walker, F.P., Schreiber, M.E., Rimstidt, J.D., 2006. Kinetics of arsenopyrite oxidative dissolution by oxygen. Geochimica et Cosmochimica Acta, 70, 1668-1676.

Wilke, M., Farges, F., Petit, P-E, Brown Jr., G.E., Martin, F., 2001. Oxidation state and coordination of Fe in minerals: An Fe K-XANES spectroscopy study. American Mineralogist, 86, 714-730.

Wilke, M., Hahn, O., Woodland, A.B., Rickers, K., 2009. The oxidation state of iron determined by Fe K-edge XANES: application to iron gall ink in historical manuscripts. Journal of Analytical Atomic Spectrometry, 24, 1364-1372.

Xia, K., Wessner, F., Bleam, W., Bloom, P.R., Skyllberg, U.L., Helmke, P.A., 1998. XANES studies of oxidation states of S in soil and aquatic humic substances. Soil Science Society of America Journal, 62, 1240-1246.

Yu, Y.M., Zhu, Y.X., Gao, Z., Gammons, C.H., Li, D., 2007. Rates of arsenopyrite oxidation by oxygen and Fe(III) at pH 1.8-12.6 and 15-45 ºC. Environental Science and Technology, 41, 6460-6464.

Zhang, Y.L., Evangelou, V.P., 1998. Formation of ferric hydroxide-silica coatings on pyrite and its oxidation behaviour. Soil Science, 163, 53-62.